SLAC–PUB–4907 Rev.
July 1989
(A)

ONLINE MONITORING OF DISPERSION FUNCTIONS AND TRANSFER MATRICES AT THE SLC*

P. EMMA, T. H. FIEGUTH, T. LOHSE
Stanford Linear Accelerator Center
Stanford University, Stanford, California 94309

ABSTRACT

The symmetries of the chromatic correction sections in the Stanford Linear Collider Final Focus System allows a high-resolution determination of the pulse-to-pulse energy fluctuations by exploiting the information from beam position monitors (BPMs) in regions of large dispersion. By correlating this signal with other BPMs, one can infer the dispersion function, as well as spatial components of transfer matrices anywhere in the arcs and the Final Focus System without interrupting the normal machine operation. We present results from data samples which were recorded during both periods of stable machine operation and periods when the linac energy was intentionally varied.

Submitted to Nuclear Instruments and Methods

⋆ Work supported by the Department of Energy, contract DE–AC03–76SF00515.

1. Introduction

The Final Focus System (FFS) [1,2] in the Stanford Linear Collider (SLC) is a complex optical system which allows strong demagnification of the beams at the interaction point. This requires not only a careful minimization of higher order aberrations using a dedicated chromatic correction section(CCS) [3] , sketched in fig. 1, but also a precise matching of the dispersion function at the entrance of the FFS. The input dispersion is measured by varying the energy in the linac and recording the correlated beam motion at strip-line beam position monitors (BPMs) in the FFS. An online matching package [4] fits the results and predicts the strengths of four corrector quadrupoles in the dispersion-matching section of the FFS. Although this is an efficient tool for dispersion *correction,* it is not suited for dispersion *monitoring* purposes because it interrupts normal machine operation and physics data-taking. In this paper, we describe a complementary scheme which allows an online nondisruptive measurement of dispersion functions by exploiting natural fluctuations of the beam energy. This allows, for the first time, monitoring of the *stability* of the dispersion match. The scheme is based on the information of CCS BPMs at positions where both dispersion and β functions are large; *i.e.,* BPMs with high sensitivity to energy and orbit fluctuations. It takes advantage of the opposite symmetry of betatron and off-energy orbits in the CCS: betatron oscillations cancel in the sum, whereas energy fluctuations cancel in the difference of the readings from two corresponding BPMs.

2. Geometric and chromatic components

We use TRANSPORT [5] notation to represent propagation of a beam from point (A) to point (B),

$$X^{(B)} = R_{11}X^{(A)} + R_{12}X'^{(A)} + R_{16}\delta \quad , \tag{1}$$

where X is the transverse beam position, X' is the beam angle with respect to the design trajectory, and δ ($\equiv \Delta p/p$) is the fractional beam momentum deviation, which we shall throughout this paper identify with the fractional energy deviation since the SLC beams are ultrarelativistic. $\mathbf{R}$ is the transfer matrix from point (A) to point (B), where we have neglected coupling between the two transverse directions X and Y.

The CCS is designed to correct lowest-order chromatic aberrations of the beam using four dipole, eight quadrupole, and eight sextupole magnets, as shown in fig. 1. These are arranged as two identical $-\mathbf{I}$ telescopes such that local geometric aberrations due to sextupoles are cancelled. Given this symmetry, the two-by-two beam transfer matrix from BPM (A) in the first telescope to BPM (B) in the second (see fig. 1) is the negative identity matrix:

$$\mathbf{R}^{(A:B)} = -\mathbf{I} \quad . \tag{2}$$

This holds for both transverse directions. For illustration, the nominal horizontal beta and dispersion functions of the FFS are shown in fig. 2. From (1) and (2), a simple relation for the beam energy deviation is found:

$$\delta = \frac{X^{(A)} + X^{(B)}}{R_{16}} \quad . \tag{3}$$

The R_{16} element from BPM (A) to BPM (B) is large and well known (460 mm), since it is almost completely determined by the two CCS dipoles B2 in fig. 1.

Transporting the dispersion at BPM (A) to BPM (B) we have:

$$\eta^{(A)} + \eta^{(B)} = R_{16} \quad , \tag{4}$$

where $\eta^{(A)}$ and $\eta^{(B)}$ are the total horizontal dispersion functions at BPMs (A) and (B), respectively. Nominally (*i.e.*, in the case of a perfect dispersion match at the entrance to

the FFS), these two values are identical (230 mm). However, *beam* dispersion, due to a mismatch upstream, will upset this equality such that the sum in (4) remains constant.

Given the equal nominal dispersion values at BPMs (A) and (B), subtraction of the two BPM signals will exactly cancel the nominal dispersive component of the beam position. We write the position at BPM (A) as the sum of a pure betatron component (independent of δ), X_β, and a pure dispersive component, then use (2) to write the position at BPM (B):

$$X^{(A)} = X_\beta + \eta^{(A)}\delta \tag{5}$$

$$X^{(B)} = -X_\beta + \eta^{(B)}\delta \quad . \tag{6}$$

Now we define ΔX as the difference between the BPMs readings:

$$\Delta X \equiv \frac{X^{(A)} - X^{(B)}}{2} = X_\beta + \Delta\eta\,\delta \quad , \tag{7}$$

where

$$\Delta\eta \equiv \frac{\eta^{(A)} - \eta^{(B)}}{2} \quad , \tag{8}$$

which represents the component of the dispersion at BPM (A) due to an upstream mismatch. In order to separate X_β from δ in (7), we assume $\Delta\eta$ is not time-dependent over a period of one set of measurements and calculate it from the correlation of δ with ΔX:

$$X_\beta = \Delta X - \frac{\langle \Delta X\,\delta \rangle}{\langle \delta^2 \rangle}\delta \quad . \tag{9}$$

The measurement of trajectory angles at BPMs (A) and (B) require the information of another pair of BPMs in the CCS, indicated by the labels (C) and (D) in fig. 1. They

are separated from BPMs (A) and (B) by simple drift spaces of known length $\Delta s \approx 2.4$ m. The angular information at BPMs (A) and (B) then becomes

$$X'^{(A)} = \frac{X^{(C)} - X^{(A)}}{\Delta s} \quad \text{and} \quad X'^{(B)} = \frac{X^{(D)} - X^{(B)}}{\Delta s} \quad , \tag{10}$$

and in analogy to (7) and (8) we derive

$$\Delta X' \equiv \frac{X'^{(A)} - X'^{(B)}}{2} = X'_\beta + \Delta\eta' \, \delta \quad , \tag{11}$$

where X'_β is the angular component of the energy uncorrelated-betatron motion and $\Delta\eta'$ is the angular dispersion mismatch at BPM (A):

$$\Delta\eta' = \frac{\eta'^{(A)} - \eta'^{(B)}}{2} \quad . \tag{12}$$

As in (9), $\Delta\eta'$ can be experimentally derived from the correlation between $\Delta X'$ and δ under the assumption that the dispersion mismatch does not change during the measurement:

$$X'_\beta = \Delta X' - \frac{\langle \Delta X' \, \delta \rangle}{\langle \delta^2 \rangle} \delta \quad . \tag{13}$$

In summary, we can measure the quantities δ, ΔX, $\Delta X'$ on a pulse-to-pulse basis. In addition, we can derive the pure energy uncorrelated betatron fluctuations X_β, X'_β from these measurements assuming that the dispersion mismatches $\Delta\eta$, $\Delta\eta'$ at BPM (A) are constant over a single period of data taking.

3. Resolution and systematic errors

The resolution of the δ signal in (3) is limited by the BPM resolutions. For the CCS, this corresponds to a value of around 20 μm. From (3) we therefore derive for the limiting resolution of δ to be $\sigma_\delta^{(res)} \approx 6 \times 10^{-5}$. This is small compared to the natural fluctuations of the beam energy which is typically of the order of 1×10^{-3}.

Several systematic errors can, in principle, affect this resolution. Possible sources include unstable dispersion-matching conditions (*e.g.,* due to orbit fluctuations in sextupoles), lattice errors in the CCS, and BPM calibration errors. All of these were analyzed quantitatively. Given the tolerances on the FFS components [6], none of these are expected to approach the value for $\sigma_\delta^{(res)}$. Systematic effects are therefore negligible.

The resolution of X_β is also limited by BPM resolutions, and slightly dependent on $|\Delta\eta|$. For all reasonable values of $|\Delta\eta|$ we find $\sigma_\beta^{(res)} < 30$ μm. The horizontal Twiss parameters at BPMs (A) and (B) are $\beta^{(A)} = \beta^{(B)} \approx 2$ km, $\alpha^{(A)} = \alpha^{(B)} \approx 300$, and therefore, given the emittance of 300 μm·μrad, a one-sigma betatron fluctuation corresponds to a position variation of ≈ 800 μm and an angular variation of ≈ 100 μrad. This provides a good X_β resolution since the BPMs are sensitive to less than 4% of the spatial betatron-size of the beam. The resolution of X'_β is worse by a factor ≈ 2 because of the relatively short drift distance of $\Delta s \approx 2.4$ m between BPMs (A) and (B).

4. BPM data acquisition

An offline FORTRAN data acquisition program has been written which gathers data from BPMs throughout the SLC and writes it to disk. The X position, Y position, and beam intensity is sampled for 850 BPMs [including the CCS BPMs (A), (B), (C), and (D)] once every few seconds. The sample rate is chosen by the user, and is typically one sample every ≈ 5 seconds. Presently data is collected interactively over short time periods where typically 100 samples are saved to a disk file for subsequent analysis. In the future, the monitoring process will run continuously, with the data stored in a circular buffer. We will also store dynamically updating moments of the BPM data which will be used for fast online fitting of lattice parameters as described in the next chapter.

5. A monitoring application

The correlation of the measured betatron fluctuations X_β and energy fluctuations δ with the position measurements of BPMs in any region of interest can be exploited for a fast measurement of the dispersion function and elements of the transfer matrix. Let $X^{(i)}$ be the beam position measured at any BPM [labelled "(i)"]. Using (1) and the definition of X_β and X'_β, we can interpret this quantity in two ways:

$$X^{(i)} = R_{11}^{(A:i)} X^{(A)} + R_{12}^{(A:i)} X'^{(A)} + R_{16}^{(A:i)} \delta \tag{14a}$$

or

$$X^{(i)} = R_{11}^{(A:i)} X_\beta + R_{12}^{(A:i)} X'_\beta + \eta^{(i)} \delta \quad . \tag{14b}$$

Both equations allow measurement of the transfer-matrix elements $R_{11}^{(A:i)}$ and $R_{12}^{(A:i)}$. The energy correlations, however, determine the *lattice* dispersion $R_{16}^{(A:i)}$ between BPMs (A) and (i) in (14a), but the dispersion *function* $\eta^{(i)}$ [*i.e.*, the total lattice dispersion between the source of energy jitter in the linac and BPM (i)] in (14b). Equation (14b) is therefore most useful for a fast judgement of the total dispersion mismatch at the entrance of the FFS, while (14a) allows the investigation of the local lattice dispersion near to the CCS and the sources of mismatches within the FFS.

In fig. 3, we present a simulation of this procedure. We generated 100 trajectories with energy fluctuations of 0.4% and relatively large betatron motions of four times the betatron size of the beam. All BPM readings were smeared according to a resolution of 20 μm. The results from properly error-weighted fits [7] to (14a) and (14b) are in good agreement with the input lattice for all BPMs inside the FFS.

Reducing the amplitude of the betatron fluctuation, however, quickly leads to numerical instabilities due to resolution limitations for many of the FFS BPMs. It is therefore

useful to reduce the number of fitted parameters in (14a) and (14b). One possibility is to average the measurements over the angular information at BPM (A):

$$\langle X^{(i)}\rangle|_{X^{(A)},\delta} = \left[R_{11}^{(A:i)} + \frac{\partial X'^{(A)}}{\partial X^{(A)}} R_{12}^{(A:i)}\right] X^{(A)} + \left[R_{16}^{(A:i)} + \frac{\partial X'^{(A)}}{\partial \delta} R_{12}^{(A:i)}\right] \delta \qquad (15a)$$

$$\langle X^{(i)}\rangle|_{X_\beta,\delta} = \left[R_{11}^{(A:i)} + \frac{\partial X'_\beta}{\partial X_\beta} R_{12}^{(A:i)}\right] X_\beta + \eta^{(i)}\delta \quad . \qquad (15b)$$

It is hence possible to measure $\eta^{(i)}$ and certain linear combinations of $R_{11}^{(A:i)}$ and $R_{12}^{(A:i)}$, or $R_{16}^{(A:i)}$ and $R_{12}^{(A:i)}$ with (15a) and (15b), respectively. The correlation parameters in these linear combinations can, in principle, be extracted from the data itself under the assumption that they are stable during a single BPM monitoring period.

Figure 4 shows as an example the correlation terms in (15a) reconstructed from a data sample taken during normal machine operation. The measurements are in good agreement with a linear combination of $R_{11}^{(A:i)}$ and $R_{12}^{(A:i)}$, or $R_{16}^{(A:i)}$ and $R_{12}^{(A:i)}$ which were obtained from fits of the nominal lattice parameters to the data and are superimposed in the figure.

Finally, averaging (15a,b) over all betatron fluctuations yields a direct relation for the dispersion function:

$$\langle X^{(i)}\rangle|_\delta = \eta^{(i)}\delta \quad . \qquad (16)$$

This simple one-parameter relation allows very stable fits. In fig. 5, we present the measurement of the dispersion function in the FFS during a period where the beam energy at the end of the linac was intentionally varied by ±0.3%. The very clean high precision measurement reveals a dispersion mismatch at the entrance of the FFS. This is confirmed in fig. 6, which shows the correlation of ΔX with δ, which according to (7) and (8) is the dispersion mismatch at BPM (A). The result of the fit is $\Delta\eta = -81$ mm ± 7 mm.

The dispersion function in the arc was derived for the same data set and is displayed in fig. 7. An example of a measurement of the FFS dispersion function during normal machine operation is presented in fig. 8. This measurement was made at a time when the dispersion was fairly well matched through the FFS. The resolution of the measurement is satisfactory although the dispersion function is derived solely from natural fluctuations in the beam energy.

This method has also been successfully tested in the damping ring to linac transport lines (RTL). There are similar optical symmetries and appropriate BPMs to provide a high resolution δ_{RTL} in both the electron and the positron RTLs. This method allows monitoring of the dispersion match at the end of the RTLs, and therefore detection of residual dispersion in the linac.

6. Present hardware limitations

At present, the range of applications for the described monitoring scheme is limited due to the fact that most of the BPMs in the arcs and the FFS are read out in a multiplexed mode. This means that only a fraction of the available BPMs will be read on exactly the same beam pulses as BPMs (A) and (B) which define the energy fluctuation via (3). This may influence the dispersion measurements in a systematic way if the natural energy fluctuations follow a fixed pattern in time. An example is shown in fig. 9 where the mean reconstructed absolute value of the dispersion [via (16)] at the arc BPMs is displayed as a function of the multiplex-channel for a data sample taken during stable machine operation. As can be seen, the measurement from channel 1 [*i.e.*, the channel on which BPMs (A) and (B) are being read out] is in good agreement with the expected value of 34 mm while all other channels show systematic deviations originating from the interference of a time-structure of the energy fluctuations with the fixed delays between adjacent pulses. Similar limitations exist for the measurements of betatron orbit

fluctuations using BPMs (A), (B), (C) and (D).

We plan to modify the software and hardware such that at least the information for BPMs (A), (B), (C) and (D) in the CCS is available on all pulses of a multiplexer scan. This will further increase the reliability and applicability of the new monitoring scheme.

7. Conclusions

Noninterfering online monitoring of dispersion functions and lattice parameters has been successfully tested at the SLC. The scheme is based on trajectory parameters measured by four BPMs in the CCS at points of large β- and η-functions. These measurements have high resolution and small systematic errors since they are insensitive to details of the CCS optics.

At present, BPM multiplexing in the arcs and FFS presents an obstacle to purely passive dispersion measurements. However, this can be overcome by BPM hardware additions and software modifications. In the future we hope to continuously read BPMs and use running moments to quickly display the FFS and arc dispersion with minimum data storage.

Acknowledgments

We acknowledge the work of P. Burchat and R. Panvini in initial feasability studies, and we thank R. Grey, N. Phinney and B. Traller for their help in setting up hardware and software. We are also indebted to A. Hutton and W. Kozanecki for their enthusiastic support and many helpful discussions. One of us (T. L.) was supported by a grant from the Max Kade Foundation.

References

[1] *SLC Design Handbook,* Stanford Linear Accelerator Center (December 1984).

[2] J. J. Murray, K. L. Brown and T. Fieguth, "The Completed Design of the SLC Final Focus System," *Proc. Particle Accelerator Conference,* Washington D.C., Vol. 3, p. 1331 (1987), SLAC–PUB–4219 (Februrary 1987).

[3] K.L. Brown, "A Conceptual Design of Final Focus Systems for Linear Colliders," SLAC–PUB–4159 (June 1987).

[4] C. M. Hawkes and P. S. Bambade, "First Order Optical Matching in the Final Focus Section of the SLAC Linear Collider," *Nucl. Inst. and Meth.* **A274** (1989) 27.

[5] K. L. Brown, F. Rothacker, D. C. Carey, and Ch. Iselin, "TRANSPORT, A Computer Program for Designing Charged Particle Beam Transport Systems," SLAC–91, Rev. 2 (May 1977), Fermilab Report No. 91, CERN 80–04.

[6] W. Kozanecki, internal note.

[7] T. Lohse, P. Emma, "Linear Fitting of BPM Orbits and Lattice Parameters," SLAC CN–371 (Februrary 1989).

Figure Captions

Fig. 1. Schematic of the chromatic correction section of the FFS. The positions of the four BPMs—(A), (B), (C) and (D)—are indicated.

Fig. 2. Nominal horizontal β function and dispersion function in the FFS. The positions of the four BPMs—(A), (B), (C) and (D)—are indicated.

Fig. 3. Reconstructed FFS lattice parameters from simulated BPM data for 100 orbits with varying energy and trajectories. The data points are the results of the fits. The solid lines are the nominal lattice parameters used for the orbit generation.

Fig. 4. Linear combinations of the FFS lattice parameters obtained from two-parameter fits to a data sample taken during normal machine operation. Superimposed (solid lines) are the best fits to the data using the nominal lattice parameters.

Fig. 5. Dispersion function in the FFS obtained from a data sample with large energy fluctuations introduced intentionally at the end of the linac. The solid line is the nominal dispersion function.

Fig. 6. Fit of the dispersion mismatch at BPM (A) for the data shown in fig. 5.

Fig. 7. Dispersion function in the north arc obtained from the data sample used in fig. 5. The nominal dispersion is indicated as a solid line.

Fig. 8. Dispersion function in the FFS from a data sample taken during normal machine operation. The solid line represents the nominal dispersion.

Fig. 9. Dependence of the average reconstructed absolute value of the arc dispersion on the BPM multiplexer channel. The data sample is identical with that used in fig. 8. The nominal value of 34 mm is also indicated.

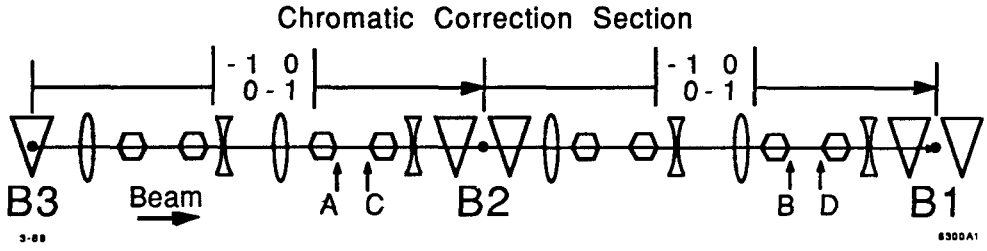

Fig. 1

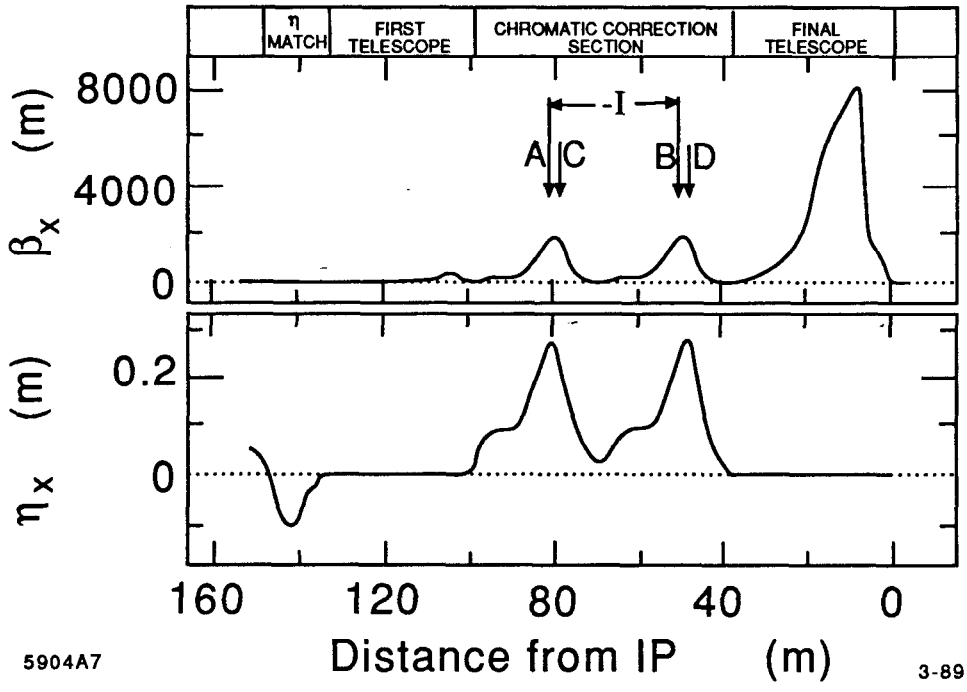
η MATCH
FIRST TELESCOPE
CHROMATIC CORRECTION SECTION
FINAL TELESCOPE
8000
4000
0
β_x (m)
-I-
A
C
B
D
0.2
0
η_x (m)
160
120
80
40
0
Distance from IP (m)
5904A7
3-89

Fig 2

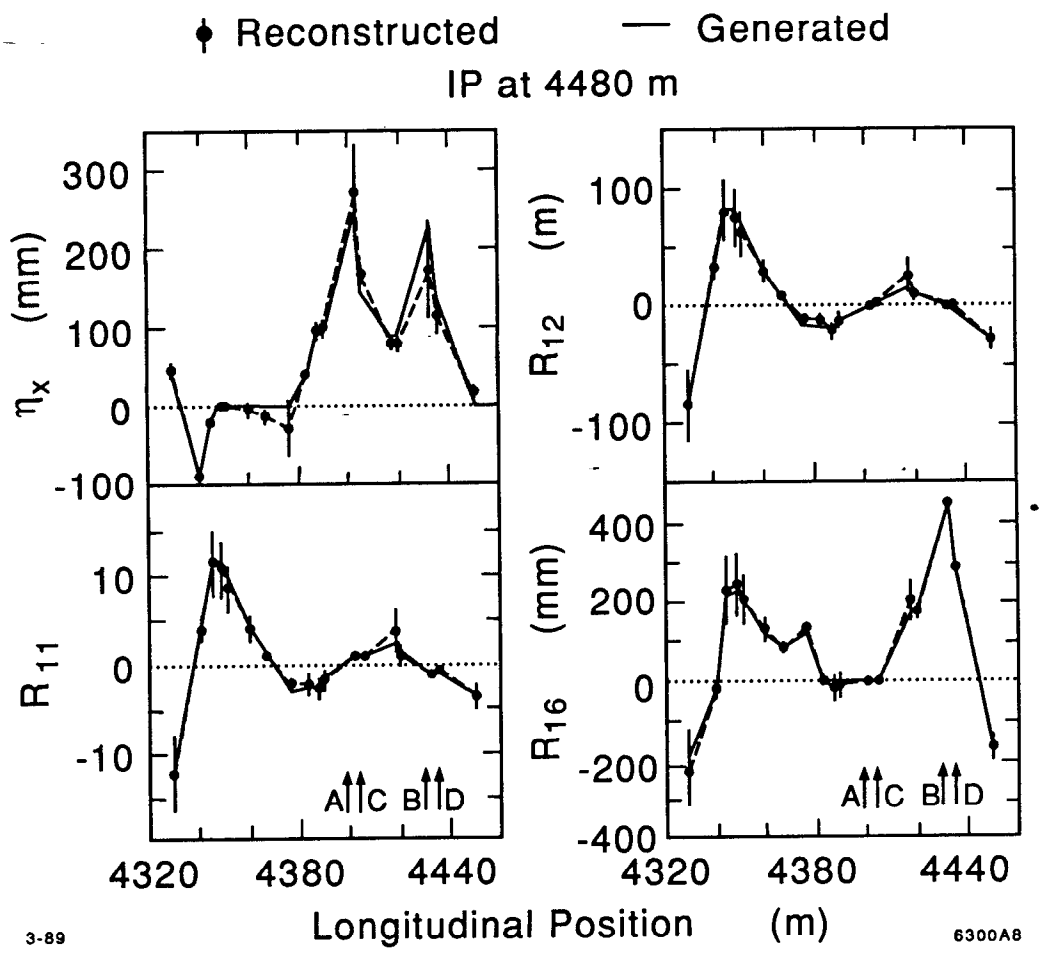
Reconstructed
Generated
IP at 4480 m
300
200
100
0
-100
η_x (mm)
100
0
-100
R_{12} (m)
10
0
-10
R_{11}
400
200
0
-200
-400
R_{16} (mm)
A C B D
A C B D
4320
4380
4440
4320
4380
4440
Longitudinal Position (m)
3-89
6300A8

Fig. 3

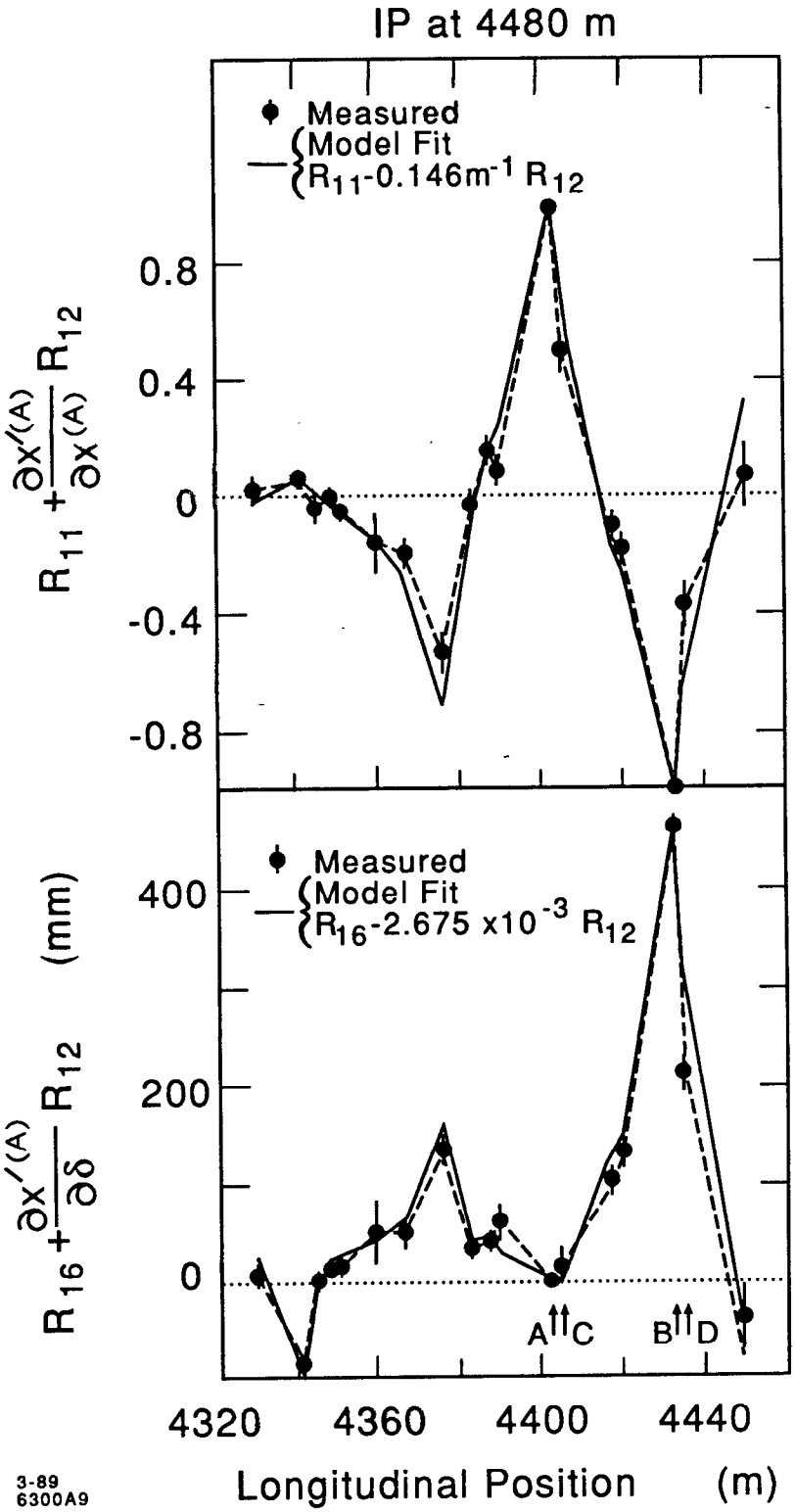
IP at 4480 m
Measured
Model Fit
R_{11}-0.146m^{-1} R_{12}
$R_{11} + \frac{\partial x'^{(A)}}{\partial x^{(A)}} R_{12}$
0.8
0.4
0
-0.4
-0.8
Measured
Model Fit
R_{16}-2.675 x10^{-3} R_{12}
$R_{16} + \frac{\partial x'^{(A)}}{\partial \delta} R_{12}$ (mm)
400
200
0
A C
B D
4320
4360
4400
4440
Longitudinal Position (m)
3-89
6300A9

Fig. 4

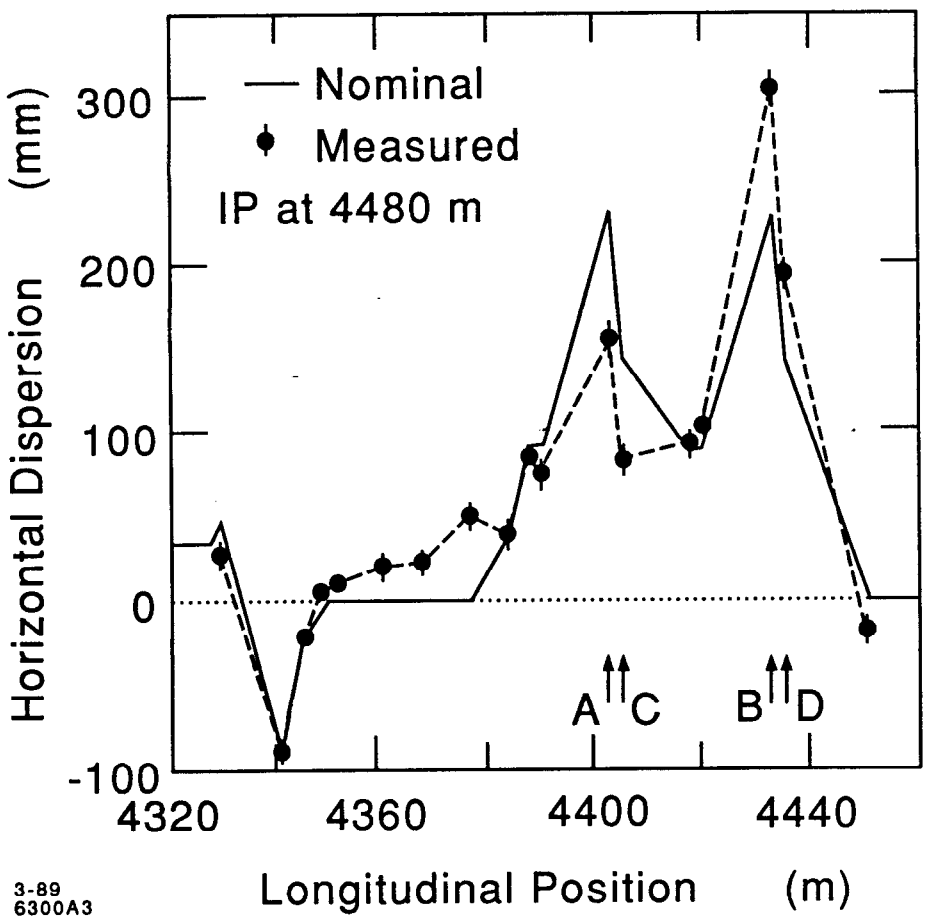
Nominal
Measured
IP at 4480 m
Horizontal Dispersion (mm)
300
200
100
0
-100
4320
4360
4400
4440
A
C
B
D
Longitudinal Position (m)
3-89
6300A3

Fig. 5

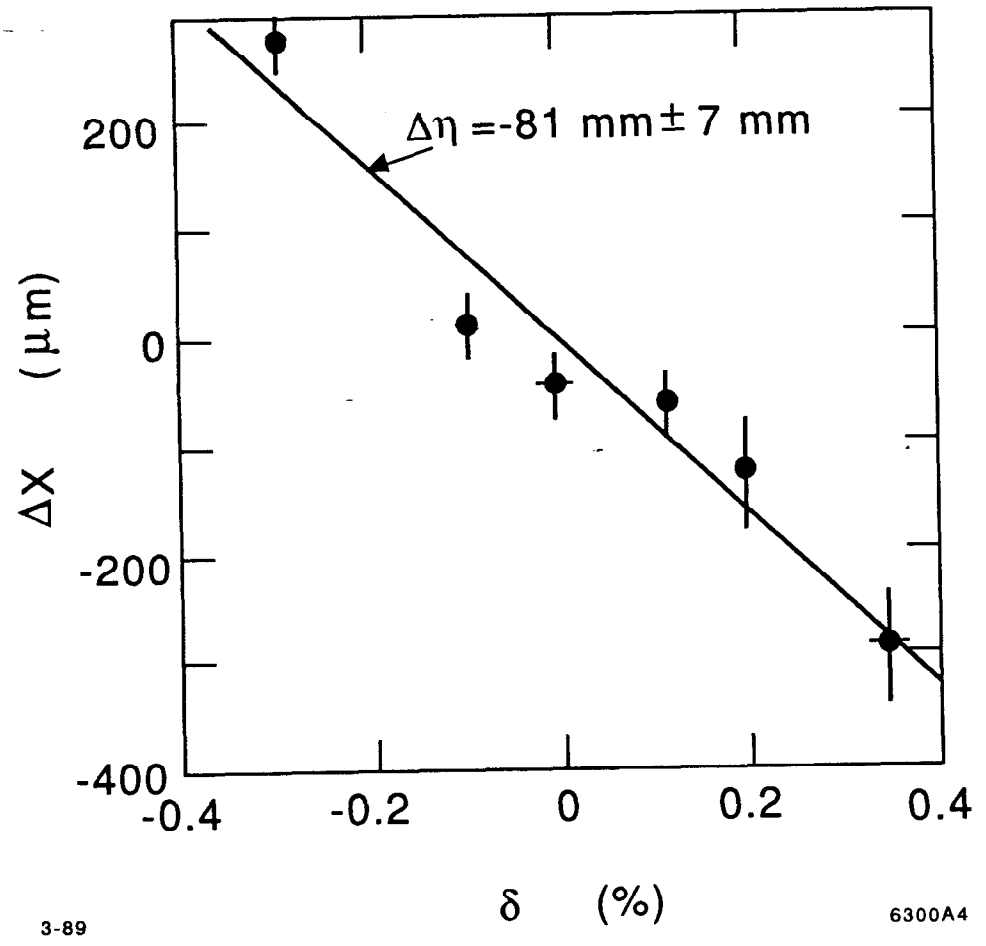

Fig. 6

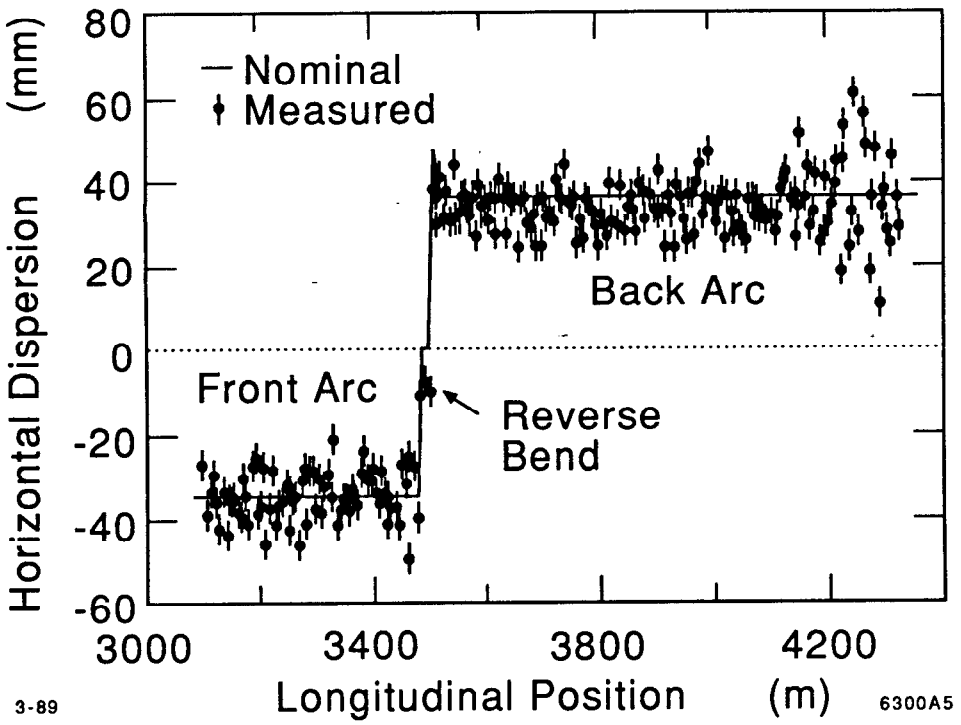
Horizontal Dispersion (mm)
80
60
40
20
0
-20
-40
-60
Nominal
Measured
Back Arc
Front Arc
Reverse
Bend
3000
3400
3800
4200
Longitudinal Position (m)
3-89
6300A5

Fig. 7

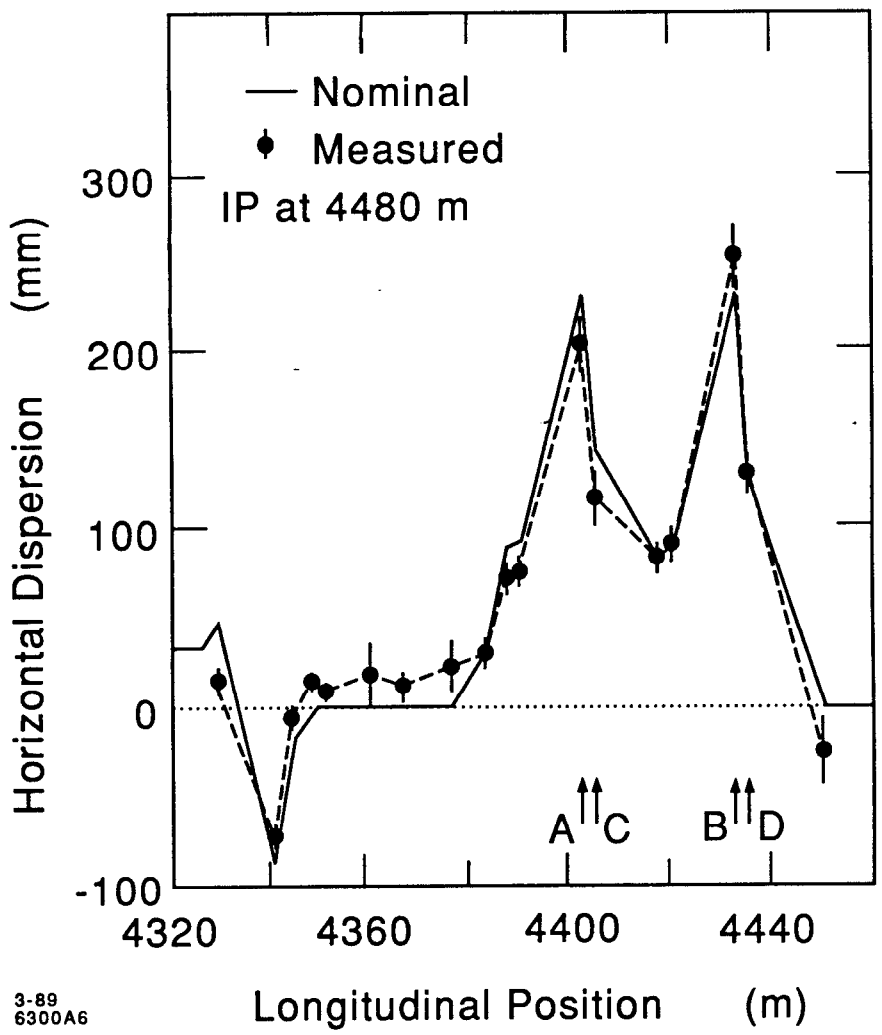
Nominal
Measured
IP at 4480 m
300
200
100
0
-100
Horizontal Dispersion (mm)
A
C
B
D
4320
4360
4400
4440
Longitudinal Position (m)
3-89
6300A6

Fig. 8

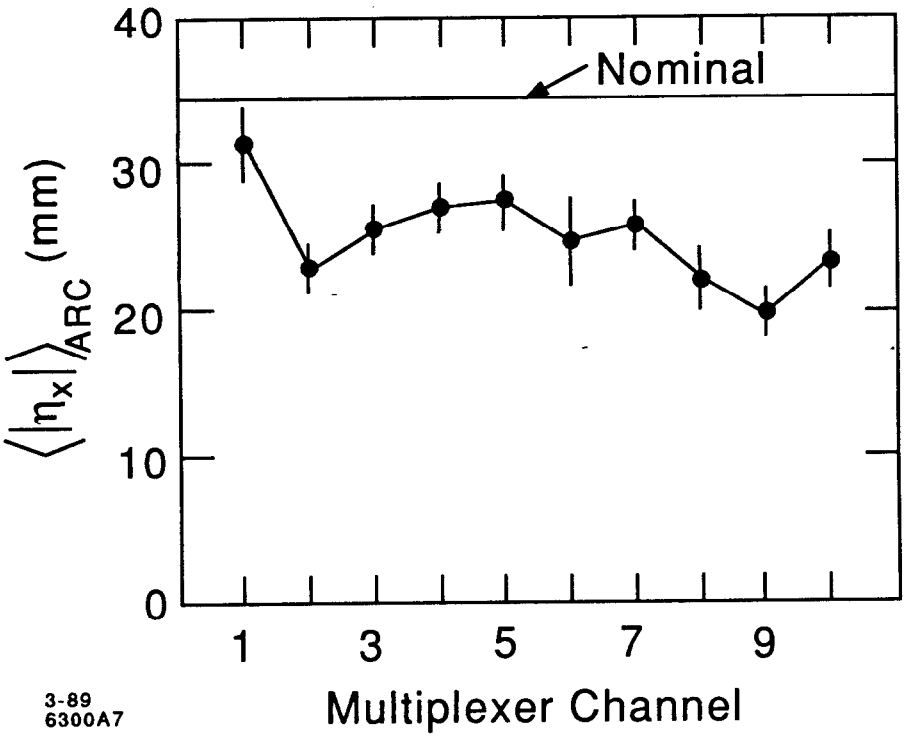
40
30
20
10
0
Nominal
$\langle |\eta_x| \rangle_{ARC}$ (mm)
1
3
5
7
9
Multiplexer Channel
3-89
6300A7

Fig. 9